Dynamics of three-particle fragmentation of $(CO_2)_2^{3+}$ ions produced by intense femtosecond laser fields

Pan Song,[1] Xiaowei Wang,[1] Congsen Meng,[1] Wenpu Dong,[1] Yongjun Li,[1] Zhihui Lv,[1] Dongwen Zhang,[1] Zengxiu Zhao,[1] and Jianmin Yuan[1,2,3,*]

[1]*Department of Physics, National University of Defense Technology, Changsha 410073, People's Republic of China*
[2]*Department of Physics, Graduate School of China Academy of Engineering Physics, Beijing 100193, People's Republic of China*
[3]*IFSA Collaborative Innovation Center, Shanghai Jiao Tong University, Shanghai 200240, People's Republic of China*

(Received 3 January 2019; revised manuscript received 8 April 2019; published 30 May 2019)

In a momentum coincidence measurement experiment, we studied the three-body fragmentation dynamics of carbon dioxide dimers in intense femtosecond laser fields. The three-dimensional momentum vectors and kinetic energies of the fragments were recorded in a cold-target recoil-ion momentum spectrometer. An analysis shows that $(CO_2)_2^{3+}$ breaks up into $CO_2^+ + CO^+ + O^+$ ions through both concerted and sequential fragmentation channels. These two fragmentation channels are consistent with the instantaneous and metastable dissociation channels in the dissociation dynamics of CO_2^{2+} ion breakup into CO^+ and O^+ ions. From Coulomb explosion imaging, our results show that, for the parallel sliding structure of the carbon dioxide dimer molecules, the angle between the C=O bond and the van der Waals bond is 48°, and the intermolecular nuclear distance $R(CO_2\text{-}CO_2)$ is 4.0 Å. By tracing the direction of the fragmentation ions, the O^+ was found to be produced from the C=O bond that is closer to the center of the C-C bond during direct dissociation. These results indicate that the dynamic characteristics of the monomer is retained and gives rise to new dynamics in the molecular cluster complexes. Finally, we have measured angular distributions of ion fragments produced by different dissociation channels of $(CO_2)_2$, and the results reveal that the structure of the dimer and its relative orientation in the laser field govern the ionization dynamics.

DOI: 10.1103/PhysRevA.99.053427

I. INTRODUCTION

For studying molecular interactions, gas molecular dimers are ideal systems because the interactions between their weak van der Waals and strong covalent bonds are complicated. The properties of one monomer are affected significantly by the presence of a neighboring molecule, despite being separated by a large nuclear distance for which their interaction would be expected to be weak. Prominent themes are charge resonance enhance ionization [1,2], interatomic Coulombic decay [3,4], and radiative charge transfer [5]. With these complicated interactions in a cluster of molecules, identifying precisely the dynamics of the many-body dissociation channel within the cluster and reconstructing the geometry of the cluster are big challenges.

Many-body fragmentation dynamics is very complicated for a chemical complex composed of polyatomic molecules. The development of coincidence measurement techniques [6,7] ensures accurate studies of many-body dissociation dynamics of molecules induced by electronic collisions [8], charged-ion collisions [9,10], or intense laser-pulse photoionization [11–14]. With the presence of Coulomb repulsive forces, the photoinduced multiply charged molecular ions are usually quite unstable and quickly fragment. Recent studies show that these molecular ions fragment into three or even more particles in both a concerted and sequential fashion [11,15–19]. Whereas the concerted fragmentation channel have all the fragmentation ions generated in a single kinetic process, the sequential breakup process evolves stepwise through an intermediate product having a certain lifetime. From a different perspective, regarding the initial state of a reaction process, the original molecular geometry is of great importance in studying the molecular dynamics. The geometric structure of molecules may be determined from experiments using electron or x-ray diffraction [20], rotational and vibrational spectroscopes [21], infrared spectrum [22–24], and Coulomb explosion imaging [25–29]. In femtosecond laser Coulomb explosion imaging, an intense laser field rapidly strips away several electrons from the molecule, and then the multiply charged molecular ion quickly breaks up, before relaxation happens in the molecular structure. Thus the instantaneous structure of the molecule may be visualized in images obtained from the three-dimensional momentum distributions of correlated fragmentation ions. However, because of the complex characteristics of the many-body fragmentation dynamics, the concerted fragmentation channel must be clarified from experiments before using the method.

In this paper, we describe experiments concerning the laser-induced triple-ionization dissociation of the van der Waals complex $(CO_2)_2$ composed of two carbon dioxide molecules. Carbon dioxide dimers have been extensively studied [30–33] after their first observation in 1961 by Bentley [34]. It is a typical system in the investigation of intermolecular interactions of nonpolar multiatomic molecules. A previous experiment claimed that the sequential fragmentation

*jmyuan@nudt.edu.cn, jmyuan@gscaep.ac.cn

channel dominates in three-body fragmentation of $(CO_2)_2^{3+}$, where the weak van der Waals bond breaks first and then one strong covalent bond [35]. A three-particle breakup of a triply ionized dimer $(CO)_2^{3+}$ ion has been reported recently by Ding *et al.* [19], who observed not only the slow dissociation of the metastable CO^{2+} in the dimer, but also a rapid dissociation that does not exist in the monomer. They found that the ultrafast dissociation is a direct consequence of the weak interaction between the two molecules in a dimer. However, in our experiment, two distinct patterns of correlated momenta of the fragments are observed and this indicates that concerted and sequential fragmentation channels both occur. As a similar system, both concerted and sequential fragmentation channels are found in the carbon dioxide dimer as well as in monomer. Furthermore, the geometry of $(CO_2)_2$ was reconstructed from the data of concerted fragmentation obtained from Coulomb explosion imaging. Both the theoretical simulations [31,36,37] and infrared spectroscopy measurements [38–45] indicate that the carbon dioxide dimer may exist as a parallel-slipped or T-shape structure. Our results show directly that $\angle CCO = 48^\circ$ and the intermolecular nuclear distance R(C-C) is 4.0 Å in the parallel-slipped structure. A clear physical image of the chemical bond breaking during concerted fragmentation was revealed by tracing the motor direction of fragment ions.

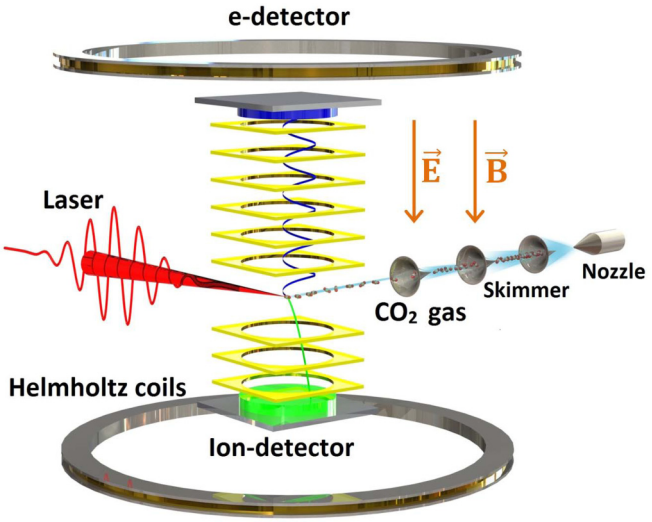

FIG. 1. Schematic diagram of a COLTRIMS used for coincidence measurements. The CO_2 dimers were generated by the supersonic expansion of CO_2 gas through a 30 μm nozzle with 8 bars backing pressure. Electrons (blue spiral) and ions (green parabola) produced by laser-induced ionization of the cold supersonic CO_2 gas jet, and detected in coincidence with the position sensitive detector consisting of microchannel plate (MCP) and delay-line anode.

II. EXPERIMENT

Our experiment was performed on the platform of a momentum spectrometer (COLTRIMS system, RoentDek, Germany) [6,7]. Dimers of the carbon dioxide molecules were generated in the supersonic expansion of CO_2 gas through a 30 μm nozzle with an 8 bars backing pressure. The linearly polarized laser pulses were centered at 790 nm with pulse duration of 25 fs and repetition rate of 10 KHz, delivered by a Ti:sapphire multipass amplification system (Femtolaser Produktions GmbH, Austria). A spherical mirror with a focal length of 75 mm focuses the laser pulses onto the molecular beam; the light intensity at the focus is estimated to be 4.5×10^{14} W/cm^2. The fragmentation ions produced by the dissociation of $(CO_2)_2$ in the laser field reach the delay line position-sensitive detector of the microchannel plate, located at the bottom of the detection chamber constrained and guided by a uniform electric field of 44 V/cm. The three-dimensional momentum of the ions can be reconstructed by the flight time and position information of the ions that are recorded by the detector. Therefore, a complete set of three-dimensional momentum vectors of the detected-ion fragments is determined (See Fig. 1.)

We concentrated on the three-particle breakup channel $(CO_2)_2^{3+} \rightarrow CO_2^+ + CO^+ + O^+$. The two-particle breakup channels, $(CO_2)_2^{3+} \rightarrow CO_2^{2+} + CO_2^+$ and $CO_2^{2+} \rightarrow CO^+ + O^+$, were selected as well for referential purposes. For the three-body fragmentation channel, three criteria were applied to select the right events from numerous experimental data. First, the events containing single ions of CO_2^+, CO^+, and O^+ were extracted; second, the sum of the momenta of the three ions must be very small to meet the requirements of momentum conservation: $|\mathbf{p}_{CO_2^+} + \mathbf{p}_{CO^+} + \mathbf{p}_{O^+}| < 10$ a.u.; third, their relative momentum is sufficiently large: $|\mathbf{p}_{CO^+} - \mathbf{p}_{O^+}| > 40$ a.u. and $|\mathbf{p}_{CO_2^+}| > 30$ a.u., to eliminate false coincidence events. The resulting fragmentation ions are considered to be correlated and come from the same $(CO_2)_2$ dimer. The events for the other two channels are selected under similar criteria.

III. RESULTS AND DISCUSSION

A. Dissociation channels

The photoion-photoion-photoion coincidence (PIPIPICO) plot of the number of correlated events of the three-particle fragmentation of CO_2 in a supersonic molecular beam induced by a strong laser field are shown in Fig. 2(a). The prominent feature along the reverse diagonal is the distribution of the correlated flight times of the different particle triples. The bright lines parallel to the coordinate axes are caused by false coincidence events of monomer ions. Applying the above filter criteria, the events corresponding to the three-particle fragmentation process $(CO_2)_2^{3+} \rightarrow CO_2^+ + CO^+ + O^+$ were extracted [Fig. 2(b)].

The momentum distribution of the fragmentation ion CO_2^+ is shown in Fig. 3(a); the black circles are experimental data. The CO_2^+ ion momenta has a relatively wide distribution with a double peak structure, suggesting that there are two mechanisms. We fit the momentum distribution of CO_2^+ ions with a sum of two Gaussian curves [blue dashed line and red solid line in Fig. 3(a)]. The central momentum and width of these two peaks are quite different. The first peak (peak I) centered at ~140 a.u. extends from ~125 a.u. to ~155 a.u., whereas the other peak (peak II) centered at ~120 a.u. extends from ~70 a.u. to ~170 a.u. From the fitted results, all the data fall under one of two peaks: the narrow peak I with 125 a.u. $< |\mathbf{p}_{CO_2^+}| < 155$ a.u.; the broader peak II with

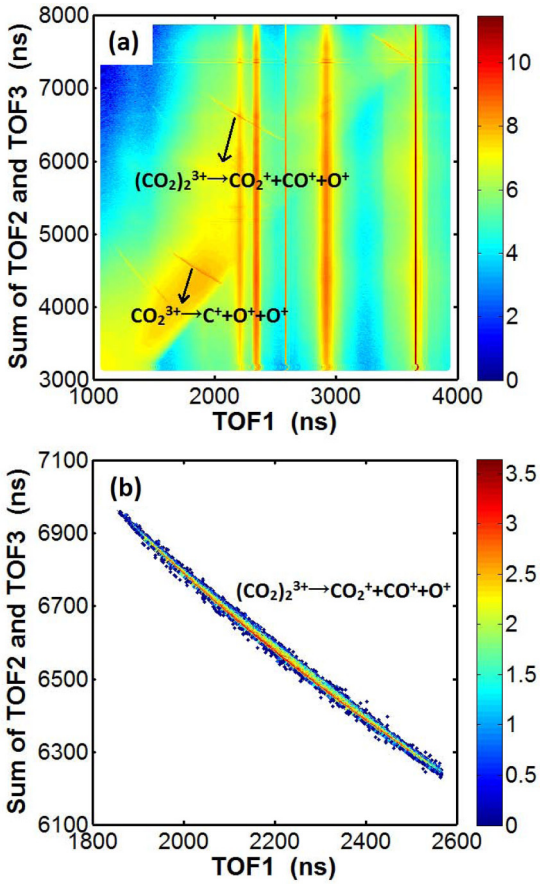

FIG. 2. Coincidence spectrum of the time of flight of three correlated fragmentation ions for CO_2 gas breakup using intense femtosecond laser field, photoion-photoion-photoion coincidence (PIPIPICO) plot. The X axis is the time of flight for the first ion, whereas the Y axis is the sum of the time of flight for the second and third ions. (a) All data of the three particle; the light intensity is 4.5×10^{14} W/cm^2. The prominent feature along the reverse diagonal is the distribution of the time of flight of the three correlated fragmentation ions. (b) Coincidence spectrum of time of flight of the three correlated fragmentation ions from dissociation channel $(CO_2)_2{}^{3+} \rightarrow CO_2{}^+ + CO^+ + O^+$. The color bar indicates the relative counts of events.

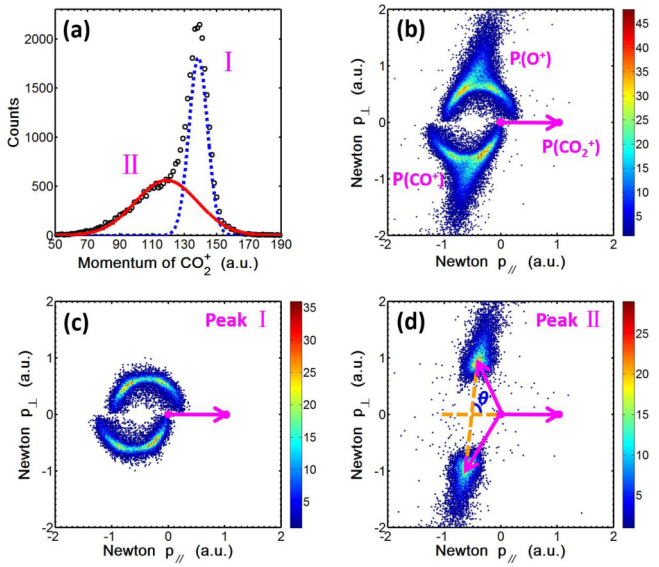

FIG. 3. (a) Momentum distribution of $CO_2{}^+$ ion: black circle line is the experimental measurement data; solid red and dashed blue curves are the two Gaussian distributions of the fit. (b) Newton diagram of all events from dissociation channel $(CO_2)_2{}^{3+} \rightarrow CO_2{}^+ + CO^+ + O^+$. (c), (d) Newton diagrams of the events corresponding to peaks I and II, respectively. The corresponding momentum of $CO_2{}^+$ ion is (c) 125 a.u. $< |\mathbf{p}_{CO_2{}^+}| <$155 a.u. and (d) $|\mathbf{p}_{CO_2{}^+}| <$125 a.u. or $|\mathbf{p}_{CO_2{}^+}| >$155 a.u.

70 a.u. $< |\mathbf{p}_{CO_2{}^+}| <$170 a.u.. Below 125 a.u. and above 155 a.u., all the data belong to the broader peak II. Between 125 a.u. and 155 a.u., peak I and peak II have significant overlap. In order to better identify the two channels, we also used the sum of kinetic energies of the CO^+ and O^+ as the limiting condition. In the following, we identify peak I as corresponding to the sequential dissociation and peak II as corresponding to the concerted fragmentation sometimes called the direct Coulomb explosion.

The 2D histogram of the momenta of the fragments in the three-particle dissociation channel [Fig. 3(b)] shows the direction of the momentum of $CO_2{}^+$, denoted $P_\parallel$ (also defines the X axis), and the momentum vector of O^+ ion, denoted $\mathbf{p}_{O^+}$, defining the positive direction of $P_\perp$. The momentum of each fragment is normalized to the momentum of the $CO_2{}^+$ ion. This plot is called the Newton diagram [46], a well-known diagram that gives explicitly the angle of the momentum vector of the correlated fragment ions in the center-of-mass coordinate system. It also helps to identify the three-body dissociation mechanism of molecular ions [10,47]. Newton diagrams for the events in peaks I and II [Figs. 3(c) and 3(d), respectively] give different distributions that indicate that these peak events have different dissociation mechanisms. In Fig. 3(c), the momentum vector distributions of the CO^+ and O^+ ions are semicircular, indicating sequential fragmentation of the $(CO_2)_2{}^{3+}$ ions for the events in peak I. In the first step, the van der Waals bond in the $(CO_2)_2{}^{3+}$ ion breaks and produces a $CO_2{}^+$ ion and a $CO_2{}^{2+}$ ion. Then the two ions fly apart under the Coulomb repulsive force; in the second step, and when the two ions are far enough apart not to affect each other, the intermediate $CO_2{}^{2+}$ ion dissociates into a CO^+ ion and an O^+ ion. The sequential fragmentation process corresponds to a ring structure in the Newton diagram, and it indicates that the angles between the momentum vectors of the three correlated fragmentation ions have changed due to the rotation of the intermediate product $CO_2{}^{2+}$ ion in the process of propagation and dissociation [10,35]. In contrast, the momentum vectors of CO^+ and O^+ are centered at certain angles relative to $CO_2{}^+$ ion for the events in peak II [Fig. 3(d)], indicating that the dissociation of the $(CO_2)_2{}^{3+}$ ion is concerted fragmentation, in which all three fragments are mutually correlated, and therefore the $CO_2{}^{2+}$ ion breaks up before the $CO_2{}^+$ ion is ejected.

The two mechanisms may be further distinguished from the energy spectra. Figure 4(a) shows the total kinetic energy released in the three-particle dimer breakup process. The dashed blue curve corresponds to peak I, the sequential breakup channel, with a peak centered on 11.8 eV; the solid

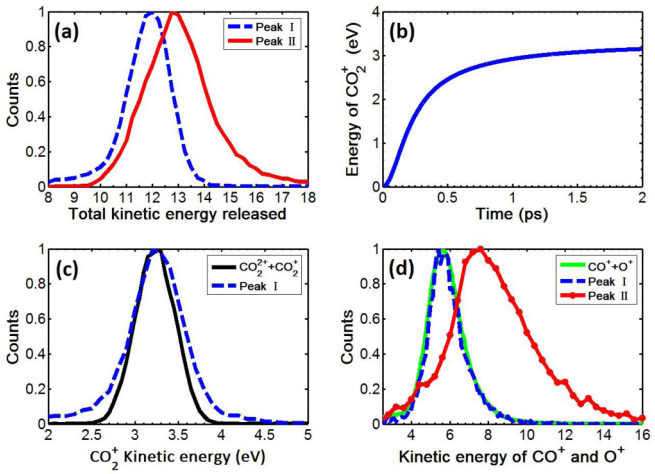

FIG. 4. (a) Total kinetic energy released in the three-particle dimer breakup process. The dashed blue curve refers to the sequential breakup channel; the solid red curve refers to the concerted fragmentation channel. (b) Kinetic energy of CO_2^+ ion in the breakup channel $(CO_2)_2^{3+} \rightarrow CO_2^{2+} + CO_2^+$ as a function of the propagation time of the ion. (c) Kinetic-energy distribution of CO_2^+. The solid blue curve corresponds to the peak I process of dimer dissociation and the dashed red curve corresponds to the breakup channel $(CO_2)_2^{3+} \rightarrow CO_2^{2+} + CO_2^+$. (d) Distribution of the sum of kinetic energies of the CO^+ and O^+. The solid blue curve indicates the obtained energy in the second step of the dimer sequential breakup (peak I); the dotted green curve corresponds to the peak II process (the same approach as for peak I); the dashed red curve corresponds to the sum of kinetic energies of the CO^+ and O^+ generated by the breakup channel $CO_2^{2+} \rightarrow CO^+ + O^+$.

red curve corresponds to peak II, the concerted fragmentation channel, with a peak centered on 12.9 eV. The two channels released different total kinetic energies. The sequential breakup channel of $(CO_2)_2^{3+}$ is further verified by analyzing its two sequential steps with each event corresponding to a two-particle breakup channel: $(CO_2)_2^{3+} \rightarrow CO_2^{2+} + CO_2^+$ and $CO_2^{2+} \rightarrow CO^+ + O^+$. To separate the energy released at the different stages of the sequential dissociation, we compared the energy released with that from the reference dissociation channels [Figs. 4(c) and 4(d)].

Assuming that the process associated with peak I corresponds to a sequential breakup, the kinetic energy of the CO_2^+ ion produced in the first step of the corresponding dimer dissociation and the CO_2^+ ion generated by the explosion channel $(CO_2)_2^{3+} \rightarrow CO_2^{2+} + CO_2^+$ should be the same. We plotted the kinetic-energy distribution of the CO_2^+ ion generated by different dissociation processes [Fig. 4(c)]. The dashed blue curve corresponds to the peak I process of the dimer dissociation and the solid black curve corresponds to the breakup channel $(CO_2)_2^{3+} \rightarrow CO_2^{2+} + CO_2^+$. The two distributions fit very well. In addition, the sum of the kinetic energies of CO^+ and O^+ obtained by dimer fragmentation in the second step should also be the same as the sum of kinetic energies of CO^+ and O^+ from the breakup channel $CO_2^{2+} \rightarrow CO^+ + O^+$. Figure 4(d) shows the distribution of the sum of the kinetic energies of CO^+ and O^+ produced by different dissociation processes; that is, the sum of the kinetic energies of CO^+ and O^+ corresponding to peaks I and II is the energy obtained by the second step of the dimer sequential breakup. The solid green curve indicates that corresponding to the explosion channel $CO_2^{2+} \rightarrow CO^+ + O^+$, and the dashed blue and the dotted red curves correspond respectively to the dissociation channels of peaks I and II of the three-particle breakup of $(CO_2)_2^{3+}$ ion. The specific kinematics requires subtracting the energy obtained from the first step of the dimer sequential breakup process from the final energy for both CO^+ and O^+ ions; that is, subtracting the kinetic energy of the CO_2^{2+} ion produced by the first step. From momentum conservation, we only need to subtract the kinetic energy of CO_2^+ ion from the sum of kinetic energies of CO^+ and O^+. To compare the energies of the two channels, we analyzed the data of concerted fragmentation in the same way as for sequential breakup, although concerted fragmentation is not a single-step process. The distribution of peak I [Fig. 4(d)] is consistent with the kinetic-energy distribution of the reference dissociation channel, but the distribution of peak II deviates from this reference distribution. Through a comparison of the distribution of the kinetic-energy release, we found that peak I in the three-particle breakup channel of $(CO_2)_2^{3+}$ ion correlates with a sequential fragmentation, whereas peak II corresponded to concerted fragmentation.

To estimate the time delay between the two steps in the sequential fragmentation channel, we simulated the dynamic process of breakup channel $(CO_2)_2^{3+} \rightarrow CO_2^{2+} + CO_2^+$ using the Coulomb potential approximation. We assumed the ion to be a point charge and the ion velocity to be zero when dissociation initiates. The length of the van der Waals bond is 4.0 Å. Figure 4(b) shows the temporal evolution of the kinetic energy of CO_2^+ ion. The kinetic energy of this fragmentation ion reaches a maximum at around 1 ps. Therefore, the lifetime of the CO_2^{2+} ion during the sequential fragmentation of dimer ions $(CO_2)_2^{3+}$ exceeds 1 ps. In addition, the ring structure of the Newton diagram [Fig. 3(c)] indicates that the time interval between the two steps of the sequential fragmentation exceeds the rotation period of the intermediate product, CO_2^{2+} [48]. However, concerted fragmentation is much faster and its dissociation time should be shorter than 1 ps.

The monomer CO_2^{2+} has been extensively investigated as a model system of a metastable molecular dissociation [49–53]. The monomer CO_2^{2+} ion breaks up through the instantaneous dissociation channel and metastable decay channel $CO_2^{2+} \rightarrow CO^+ + O^+$ [51], both with significantly different dissociation times. The lifetime of these metastable decays of CO_2^{2+} ion ranges from a few microseconds to tens of microseconds [48,52–55]. For the instantaneous dissociation channel, its dissociation time is difficult to observe because the time window is limited. However, Wu *et al.* [51] observed an anisotropic angular distribution of the CO^+ and O^+ ions in the experiment that results from an instantaneous dissociation channel in the intense femtosecond laser fields. The dissociation time is approximately 400 fs. In terms of dissociation time, the two three-particle breakup channels of $(CO_2)_2^{3+}$ ions are consistent with the instantaneous dissociation channel and the metastable decay channel of the monomer CO_2^{2+} ions. That is, the sequential dissociation of the dimer is caused by the metastable decay of the monomer CO_2^{2+} ions,

whereas the concerted fragmentation channel of the dimer is essentially an instantaneous dissociation of monomer CO_2^{2+} ions. This indicates that the CO_2^{2+} ions retain the dynamic characteristic of the monomer ions when they are placed in equilibrium with the cations of a van der Waals complex. For the metastable decay, Hogreve *et al.* [56] noted that a tunneling is required through a potential barrier on the potential-energy surface of the ground electronic state $^3\Sigma_g^-$ of the CO_2^{2+} ion. Sharma *et al.* [55] calculated the dynamic process of the CO_2^{2+} ion in the electronic ground state using a time-dependent quantum-mechanics method and they found states with lifetimes of greater than 7 ps. A more important reason is slow intersystem crossing transitions from an excited state to the triple state of the ground state and then a rapid dissociation in the ground state [52]. As illustrated in Fig. 3(a), the area of the two peaks represents the branching ratio of the two dissociation channels. The ratio of the sequential breakup to the concerted fragmentation is about 3:2. Their ratio is close to 1:1 with a considerable overlap of the two peaks. In other words, the branching ratio of metastable dissociation and instantaneous dissociation is 1:1. These results demonstrate that the probability of an instantaneous dissociation channel and a metastable decay channel is almost the same when the CO_2^{2+} ion is placed in the equilibrium cations of a van der Waals complex. This is a consequence of the weak intermolecular interaction in the dimer. The more essential reason is the probability of metastable and fast dissociation state is almost equal in the molecular vibration state caused by laser ionization.

The measured energy released was 5.5 eV for the CO_2^{2+} breakup into $CO^+ + O^+$ ions in sequential fragmentation and is close to the energy released (5.2 eV) for the ground-state dissociation of the monomer CO_2^{2+}. It follows that the breakup of CO_2^{2+} is dissociated along the ground-state potential-energy curve in the sequential fragmentation. In Fig. 5, three sets of potential-energy curves for the $CO^+ + O^+$ interaction are given to help understand the dissociation processes. The blue line is the ground-state potential curve of CO_2^{2+} obtained using *ab initio* calculations, the red line is the pure Coulomb potential of two point charges, the violet curve is the ground-state potential curve of CO_2 molecule, and the green curve is the sum of the red and violet lines. The blue line gives the fully relaxed $CO^+ + O^+$ interaction after double ionization; the green line gives approximately the $CO^+ + O^+$ interaction without electronic relaxation after double ionization. The pure Coulomb potential can be used to represent the $CO^+ + O^+$ interaction beyond 2.2 Å, where the covalent interaction is negligible. Without electronic excitations, the actual $CO^+ + O^+$ interaction potential curve after double ionization should be between the green and blue lines with a potential barrier of less than 2 eV at around 1.8 Å. If we assume the nuclear vibrational wave function does not change during the electronic ionizations, the nuclear vibrational state after ionization should be a superposition of the ground state and a few excited vibrational states. Therefore, the 5.5 eV measured dissociation energy of the CO_2^{2+} ion is slightly higher than its ground-state dissociation energy 5.2 eV. The dissociation process of the CO_2^{2+} ion is a quantum tunneling effect through the potential barrier and the subsequent Coulomb explosion. Because the potential barrier is low and narrow, quantum tunneling of excited nuclear vibrational states is very fast and detected in the experiment as a concerted Coulomb explosion of the three charged particles. The quantum-tunneling rate of the ground nuclear vibrational state is low and the complete decay of the state needs a much longer time which has been detected in experiment as sequential fragmentation. The measured ratio between the concerted Coulomb explosion and sequential fragmentation for the $(CO_2)_2$ are normally different from that for the CO_2 molecule.

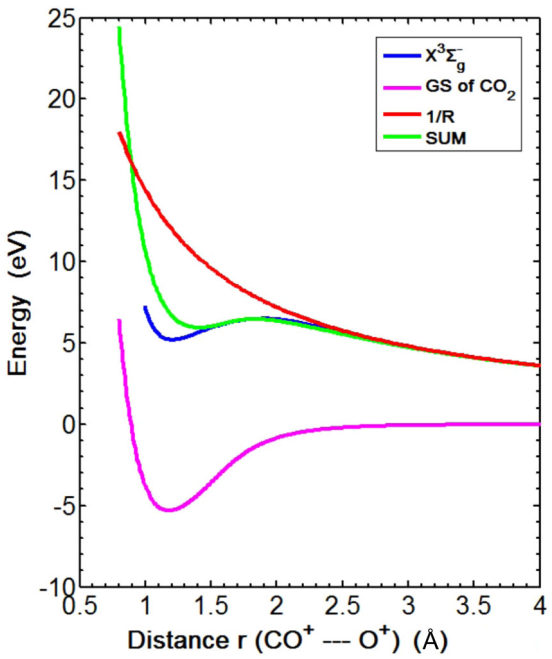

FIG. 5. Potential-energy curve of the CO_2^{2+} ion, where r is the distance between the center of mass CO^+ and O^+. The blue and red lines correspond to the potential-energy curve of the ground state $X\,^3\Sigma_g^-$ and the Coulomb potential curve $1/R$, respectively. The potential-energy curve of ground-state $X\,^3\Sigma_g^-$ comes from Ref. [57]. The violet line represents the ground-state potential-energy curve of the carbon dioxide molecule; the green curve is the sum of red and violet lines.

B. Geometry of the dimer and the angular distribution of the fragment ions

In addition, we reconstructed the geometry of the carbon dioxide dimer molecule from the concerted fragmentation of the dimer. Many theoretical calculations show that the carbon dioxide dimer exists in two forms: a parallel-slipped structure and a T-shape structure. However, the structures observed are different because dimers are produced in different ways in the experiments having mainly infrared spectra [38–45]. However, the parallel-slipped structure of the carbon dioxide dimer (Fig. 6) was only observed in the adiabatic expansion of the ultrasonic molecular beam [38,40]. In the gas phase, the most stable structure of the carbon dioxide dimer is the nonpolarized parallel-slipped structure [42]. They obtained for ∠CCO an angle of around 60° between the van der Waals

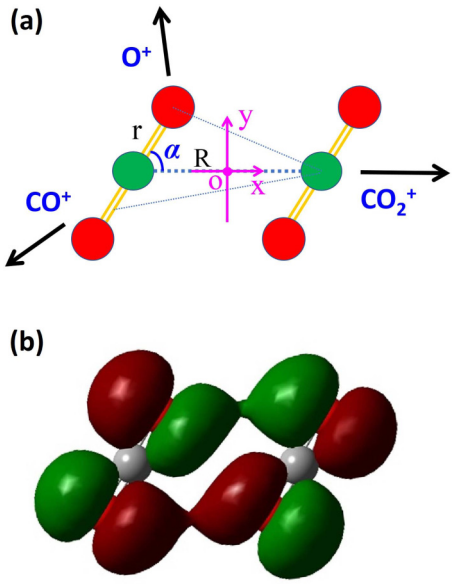

FIG. 6. Parallel-slipped structure of the carbon dioxide dimer. (a) We set up a plane rectangular coordinate system with the geometric center of the dimer molecule as origin. R is the distance between the two carbon dioxide molecules, r is the length of the C=O bond, and α is the angle between the broken C=O bond during concerted fragmentation and the van der Waals bond. (b) Schematic diagram of the HOMO orbitals of the dimer molecule.

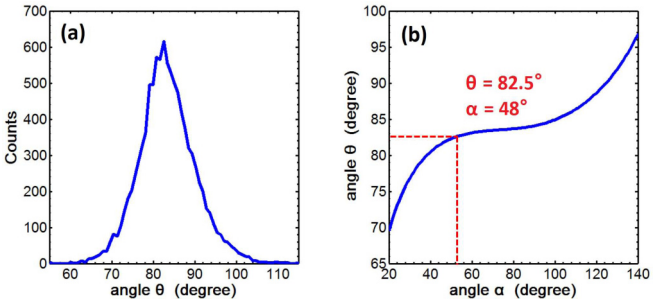

FIG. 7. (a) Experimentally measured angle between the momentum of the final state of the three correlated fragmentation ions generated through concerted fragmentation. (b) Simulated relationship between angle θ and angle α between the van der Waals bond and the C=O bond by using the Coulomb potential model $\theta = 82.5^\circ$ corresponds to $\alpha = 48^\circ$.

bond (C-C) and the covalent bond (C=O); the intermolecular distance R(C-C) is about 3.6 Å. From Fig. 4(d), the kinetic energy released in a single peak structure indicates that the dissociation occurs in a particular electron state [51]. However, CO_2^{2+} ion dissociates into CO^+ and O^+ ions in a variety of electron states [57,58]. To simplify the model, we assumed concerted fragmentation of the dimer in producing the dynamics of the fragmentation ions and simulated the process using the Newton iteration method applied to the Coulomb potential model. When applying the intense femtosecond laser fields, we assumed the dimer molecules quickly lose three electrons and the three fragmentation ions are generated rapidly subject to Coulomb repulsive forces. The initial velocity of each ion is zero and the Coulomb repulsion force of the other two ions is applied to the motion simultaneously. We set up a plane rectangular coordinate system with the geometric center of the dimer molecule as origin, as shown in Fig. 6(a). We obtained the intermolecular nuclear distance between two CO_2 is 4.0 Å by breakup channels $(CO_2)_2^{3+} \rightarrow CO_2^{2+} + CO_2^+$. We subtract the energy released by the van der Waals bond breakup from the total energy released in the concerted fragmentation process to obtain the energy released by the C=O bond breakup. The initial bond length r is 2.2 Å, determined by $E = 1/r$, where r is the distance between the center of mass CO^+ and O^+. The simulation time was set long enough to ensure the three fragmentation ions were far enough apart and the initial potential energy was converted into the final kinetic energy of the fragmentation ions. In the experiments, we measured the angle θ between the momentum of the final state of the three correlated fragmentation ions generated through concerted fragmentation [Fig. 3(d)]. The results of the angle statistics are shown in Fig. 7(a). We simulated the functional relationship between angle θ and angle $\angle$CCO [marked as α in Fig. 6(a)] between the van der Waals bond and the C=O bond using the Coulomb potential model [Fig. 7(b)]. We set the dimer angle α from zero to 180° with increments of 0.5° and for each α the angle θ between the momenta of the three fragmentation ions were obtained, as shown in Fig. 7(b). From the results of our experimental measurements, $\theta = 82.5^\circ$ corresponding to $\alpha = 48^\circ$ and R(C-C) = 4.0 Å.

In addition, our data show evidence of the fragmentation ion O^+ coming from the side $\alpha < 90^\circ$, with α being the angle between the broken C=O bond and the van der Waals bond. That is, the weak interaction affects the breakup of the C=O bond pointing to the carbon dioxide nearby. In the carbon dioxide dimer, the van der Waals bond affects the strong-field ionization processes via its role in the geometric conformation. The van der Waals bond coupling the two carbon dioxide molecules together form a relatively stable parallel sliding structure in our experimental conditions and hence the shape of the molecular orbital of dimer is determinate and affects the ionization probability. A schematic diagram of the HOMO orbitals of the dimer molecule are shown in Fig. 6(b) (GAUSSIAN09, MP2 combine cc-pvqz) using red and green to distinguish the two degenerate orbitals on the two sides of C atoms. Because of the much larger ionization potential for ionizing of the second electron from the same molecular orbital, the double ionization is most likely to happen with two electrons being ionized from two well-separated orbitals of different colors in the pair of carbon dioxide molecules. This can be found in the following angular distribution of the $(CO_2)_2^{2+} \rightarrow CO_2^+ + CO_2^+$ dissociation. The positive charges left by the two ionized electrons are localized on the outermost covalent (C=O) bonds of the two molecules and prompt a third ionized electron from the inner side covalent (C=O) bond of one of the carbon dioxide molecules. The strong combination of Coulomb repulsive forces from both sides draws the O^+ ion closer to the geometric center of the dimer, which then dissociates from the molecule.

It is well known that the ionization of a molecule in an intense laser field usually depends on the orientation of the molecular axis relative to the laser field [1,2,59–65]. The orientation-dependent strong-field ionization of a cluster

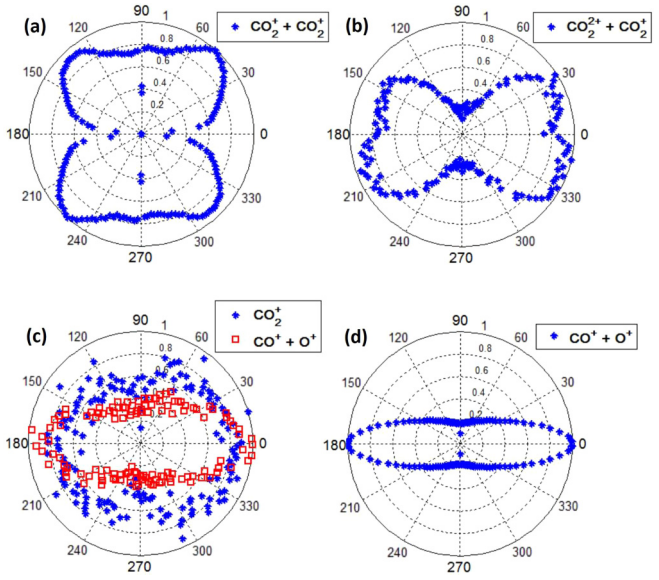

FIG. 8. Angular distributions of fragmentation ions generated by different breakup channels in our linearly polarized light. (a) For $(CO_2)_2^{2+} \rightarrow CO_2^+ + CO_2^+$. (b) For $(CO_2)_2^{3+} \rightarrow CO_2^{2+} + CO_2^+$. (c) $CO_2^{2+} \rightarrow CO^+ + O^+$. (d) The angular distributions of the ion pair (CO^+, O^+) (red square) and the CO_2^+ ion (blue point) for $(CO_2)_2^{3+} \rightarrow CO_2^+ + CO^+ + O^+$.

of N_2Ar has been reported previously by Wu *et al.* [66], who observed that the orientations of different bonds with respect to the laser field polarization vectors alter their roles in producing various channels. We discuss the correlation of the structure of the carbon dioxide dimer to its relative orientation dependent ionization in the laser field. In Fig. 8, we plot the angular distributions of fragmentation ions generated by different breakup channels in our linearly polarized light. The multiple ionizations of molecules can be produced by both sequential field ionization as well as nonsequential recollision ionization. Multiple field ionization occurs most likely on different site nearly degenerate orbitals, while the recollision ionization can happen on the same site or different site orbitals depending on the collisional ionization cross sections of the corresponding orbital. The angular distribution of fragmentation ions generated by the Coulomb explosion channel $(CO_2)_2^{2+} \rightarrow CO_2^+ + CO_2^+$ is shown in Fig. 8(a); its peak value is around 50°. The double ionizations occur on two different molecules in the dimer and are most likely direct laser field ionizations. The results show that the dissociative double ionization probability is highest when the angle between the orientation of the van der Waals bond and the polarization direction of the laser field is 50°. The angle between the van der Waals bond and the C=O bond that we obtained above is 48°, and the result from this angular distribution indicates that the occurrence of the dissociative double ionization is dominated when the carbon dioxide molecules in the dimer are distributed along the axial direction of the laser polarization. In this instance, the final dissociation occurs from the two-site double ionization of the carbon dioxide dimers. The angular distribution peak of fragmentation ions generated by the breakup channel $(CO_2)_2^{3+} \rightarrow CO_2^{2+} + CO_2^+$ is around 20°, and there is a considerable distribution around 0° [Fig. 8(b)]. In this case the double ionizations of the CO_2^{2+} ion cannot be on both sides of the C atom and are most likely produced by the recollision ionization of two electrons from the same side of the CO_2 molecule. As is seen from the molecular orbital of Fig. 6(b), one potential scenario of electron ejection is to order one field ionized electron from each of the C=O bond sites of the two molecules that is farthest from the geometric center of the dimer, and a third electron ionized from one of the same two C=O bonds by recollision of one of the field ionized electrons. Figure 8(c) shows the angular distribution of fragmentation ions generated by concerted fragmentation of the three-body breakup channel $(CO_2)_2^{3+} \rightarrow CO_2^+ + CO^+ + O^+$. In this case, the triple ionizations occur on three different bonds and could be produced by both sequential field ionization and nonsequential recollision ionization. We showed the relative momenta of the ion pair (CO^+, O^+) and the departing CO_2^+. The angular distributions of the ion pair (CO^+, O^+) and the CO_2^+ ion show that the concerted three-body breakup is mostly created with the covalent bond (C=O) along the polarization direction of the laser field. For our linearly polarized light, the angular distribution is distributed along the laser polarization of fragmentation ions generated by the dissociative double ionization channel $CO_2^{2+} \rightarrow CO^+ + O^+$ of the monomer carbon dioxide; see Fig. 8(d). The results reveal that the orientation of the covalent bond of carbon dioxide contained in the dimer parallel to the laser field dominates the concerted fragmentation.

IV. CONCLUSION

Our results suggest that triple-ionization-induced three-body breakup of carbon dioxide dimers by intense femtosecond laser beam occurs through two mechanisms: the sequential fragmentation and concerted breakup. For the sequential fragmentation, the van der Waals bond of $(CO_2)_2^{3+}$ ion was first broken up to generate the CO_2^+ ion and the intermediate CO_2^{2+} ion, and then the CO_2^{2+} ion further dissociates to produce the CO^+ and O^+ ions. In a concerted breakup, the van der Waals inter- and covalent bonds C=O break simultaneously; the $(CO_2)_2^{3+}$ ion almost produces three fragmentation ions at the same time. We propose that the origin of the two channels arises from the instantaneous dissociation and metastable decay of CO_2^{2+}. This implies that the CO_2^{2+} ions retain the dynamic characteristic of the monomer ions when placed with equilibrium cations of a van der Waals dimer. Nevertheless, the ratio of the two channels changes as a consequence of the weak intermolecular interaction in the dimer. Given the rates of concerted fragmentation, we simulated the dynamics of the fragmentation ions using the Coulomb potential model. We obtained a clear structure of the carbon dioxide dimer molecules, specified by $\alpha = 48°$, and R(C-C) = 4.0 Å. Simulations showed that simultaneous with the breaking of the van der Waals bond during a concerted Coulomb explosion is the breaking of the covalent bond (C=O) pointing to the nearest carbon dioxide molecule. That is, a weak interaction affects this breakup.

ACKNOWLEDGMENT

Z.Z. acknowledges support from the Major Research plan of National Natural Science Foundation of China under Grant

No. 91850201. D.Z. acknowledges support from the NSAF Joint Fund No. U1830206. C.M. acknowledges support from the National Natural Science Foundation of China under Grant No. 1160040015. Z.L. acknowledges support from the National Natural Science Foundation of China under Grant No. 11574396.

[1] T. Zuo and A. D. Bandrauk, Phys. Rev. A **52**, R2511 (1995).
[2] J. Wu, M. Meckel, L. P. H. Schmidt, M. Kunitski, S. Voss, H. Sann, H. K. Kim, T. Jahnke, A. Czasch, and R. Dorner, Nat. Commun. **3**, 1113 (2012).
[3] T. Jahnke, A. Czasch, M. S. Schöffler, S. Schössler, A. Knapp, M. Käsz, J. Titze, C. Wimmer, K. Kreidi, R. E. Grisenti, A. Staudte, O. Jagutzki, U. Hergenhahn, H. Schmidt-Böcking, and R. Dörner, Phys. Rev. Lett. **93**, 163401 (2004).
[4] T. Havermeier, T. Jahnke, K. Kreidi, R. Wallauer, S. Voss, M. Schöffler, S. Schössler, L. Foucar, N. Neumann, J. Titze, H. Sann, M. Kühnel, J. Voigtsberger, J. H. Morilla, W. Schöllkopf, H. Schmidt-Böcking, R. E. Grisenti, and R. Dörner, Phys. Rev. Lett. **104**, 133401 (2010).
[5] N. Saito, Y. Morishita, I. H. Suzuki, S. D. Stoychev, A. I. Kuleff, L. S. Cederbaum, X. J. Liu, H. Fukuzawa, G. Prumper, and K. Ueda, Chem. Phys. Lett. **441**, 16 (2007).
[6] J. Ullrich, R. Moshammer, R. Dorner, O. Jagutzki, V. Mergel, H. Schmidtbocking, and L. Spielberger, J. Phys. B **30**, 2917 (1997).
[7] R. Dorner, V. Mergel, O. Jagutzki, L. Spielberger, J. Ullrich, R. Moshammer, and H. Schmidtbocking, Phys. Rep. **330**, 95 (2000).
[8] E. Wang, X. Shan, Z. Shen, X. Li, M. Gong, Y. Tang, and X. Chen, Phys. Rev. A **92**, 062713 (2015).
[9] J. Matsumoto, A. Leredde, X. Flechard, K. Hayakawa, H. Shiromaru, J. Rangama, C. L. Zhou, S. Guillous, D. Hennecart, T. Muranaka, A. Mery, B. Gervais, and A. Cassimi, Phys. Rev. Lett. **105**, 263202 (2010).
[10] N. Neumann, D. Hant, L. P. H. Schmidt, J. Titze, T. Jahnke, A. Czasch, M. S. Schöffler, K. Kreidi, O. Jagutzki, H. Schmidt-Böcking, and R. Dörner, Phys. Rev. Lett. **104**, 103201 (2010).
[11] X. Gong, M. Kunitski, L. P. H. Schmidt, T. Jahnke, A. Czasch, R. Dörner, and J. Wu, Phys. Rev. A **88**, 013422 (2013).
[12] X. Gong, Q. Song, Q. Ji, H. Pan, J. Ding, J. Wu, and H. Zeng, Phys. Rev. Lett. **112**, 243001 (2014).
[13] A. De Fanis, M. Oura, N. Saito, M. Machida, M. Nagoshi, A. Knapp, J. Nickles, A. Czasch, R. Dorner, Y. Tamenori *et al.*, J. Phys. B **37**, L235 (2004).
[14] U. Ablikim, C. Bomme, H. Xiong, E. Savelyev, R. Obaid, B. Kaderiya, S. Augustin, K. Schnorr, I. Dumitriu, T. Osipov *et al.*, Sci. Rep. **6**, 38202 (2016).
[15] M. R. Jana, P. N. Ghosh, B. Bapat, R. K. Kushawaha, K. Saha, I. A. Prajapati, and C. P. Safvan, Phys. Rev. A **84**, 062715 (2011).
[16] R. K. Singh, G. S. Lodha, V. Sharma, I. A. Prajapati, K. P. Subramanian, and B. Bapat, Phys. Rev. A **74**, 022708 (2006).
[17] E. Wang, X. Shan, Z. Shen, M. Gong, Y. Tang, Y. Pan, K.-C. Lau, and X. Chen, Phys. Rev. A **91**, 052711 (2015).
[18] C. Wu, C. Wu, Y. Fan, X. Xie, P. Wang, Y. Deng, Y. Liu, and Q. Gong, J. Chem. Phys. **142**, 124303 (2015).
[19] X. Ding, M. Haertelt, S. Schlauderer, M. S. Schuurman, A. Y. Naumov, D. M. Villeneuve, A. R. W. McKellar, P. B. Corkum, and A. Staudte, Phys. Rev. Lett. **118**, 153001 (2017).
[20] A. O. Er, J. Chen, and P. M. Rentzepis, J. Appl. Phys. **112**, 031101 (2012).
[21] T. Ogata, W. Jager, I. Ozier, and M. C. L. Gerry, J. Chem. Phys. **98**, 9399 (1993).
[22] Y. Xu and A. R. W. Mckellar, Mol. Phys. **88**, 859 (1996).
[23] H. Shanks, C. J. Fang, L. Ley, M. Cardona, F. J. Demond, and S. Kalbitzer, Phys. Status Solidi B **100**, 43 (1980).
[24] C. E. Dinerman and G. E. Ewing, J. Chem. Phys. **53**, 626 (1970).
[25] Z. Vager, R. Naaman, and E. P. Kanter, Science **244**, 426 (1989).
[26] K. Ueda, A. De Fanis, N. Saito, M. Machida, K. Kubozuka, H. Chiba, Y. Muramatu, Y. Sato, A. Czasch, O. Jaguzki *et al.*, Chem. Phys. **289**, 135 (2003).
[27] A. Hishikawa, H. Hasegawa, and K. Yamanouchi, Chem. Phys. Lett. **388**, 1 (2004).
[28] S. Chelkowski, P. B. Corkum, and A. D. Bandrauk, Phys. Rev. Lett. **82**, 3416 (1999).
[29] M. Pitzer, M. Kunitski, A. S. Johnson, T. Jahnke, H. Sann, F. Sturm, L. Schmidt, H. Schmidtbocking, R. Dorner, J. Stohner *et al.*, Science **341**, 1096 (2013).
[30] R. E. Leckenby and E. J. Robbins, Proc. R. Soc. London A **291**, 389 (1966).
[31] R. Bukowski, J. Sadlej, B. Jeziorski, P. Jankowski, K. Szalewicz, S. A. Kucharski, H. L. Williams, and B. M. Rice, J. Chem. Phys. **110**, 3785 (1999).
[32] K. W. Jucks, Z. S. Huang, D. Dayton, R. E. Miller, and W. J. Lafferty, J. Chem. Phys. **86**, 4341 (1987).
[33] A. E. Barton, A. Chablo, and B. J. Howard, Chem. Phys. Lett. **60**, 414 (1979).
[34] P. G. Bentley, Nature (London) **190**, 432 (1961).
[35] Y. Fan, C. Wu, X. Xie, P. Wang, X. Zhong, Y. Shao, X. Sun, Y. Liu, and Q. Gong, Chem. Phys. Lett. **653**, 108 (2016).
[36] J. D. Mcmahon and J. R. Lane, J. Chem. Phys. **135**, 154309 (2011).
[37] R. Eggenberger, S. Gerber, and H. Huber, Mol. Phys. **72**, 433 (1991).
[38] M. Dehghany, A. R. W. Mckellar, M. Afshari, and N. Moazzenahmadi, Mol. Phys. **108**, 2195 (2010).
[39] N. Moazzenahmadi and A. R. W. Mckellar, Int. Rev. Phys. Chem. **32**, 611 (2013).
[40] X. Xie, C. Wu, Y. Liu, W. Huang, Y. Deng, Y. Liu, Q. Gong, and C. Wu, Phys. Rev. A **90**, 033411 (2014).
[41] L. M. Nxumalo and T. A. Ford, J. Mol. Struct. **327**, 145 (1994).
[42] A. Schriver, L. Schrivermazzuoli, and A. A. Vigasin, Vibrat. Spectrosc. **23**, 83 (2000).
[43] L. Mannik, J. C. Stryland, and H. L. Welsh, Can. J. Phys. **49**, 3056 (1971).
[44] M. A. Walsh, T. H. England, T. R. Dyke, and B. J. Howard, Chem. Phys. Lett. **142**, 265 (1987).
[45] K. W. Jucks, Z. S. Huang, R. E. Miller, G. T. Fraser, A. S. Pine, and W. J. Lafferty, J. Chem. Phys. **88**, 2185 (1988).

[46] Y. Muramatsu, K. Ueda, N. Saito, H. Chiba, M. Lavollée, A. Czasch, T. Weber, O. Jagutzki, H. Schmidt-Böcking, R. Moshammer, U. Becker, K. Kubozuka, and I. Koyano, Phys. Rev. Lett. **88**, 133002 (2002).
[47] C. Wu, C. Wu, D. Song, H. Su, Y. Yang, Z. Wu, X. Liu, H. Liu, M. Li, Y. Deng, Y. Liu, L.-Y. Peng, H. Jiang, and Q. Gong, Phys. Rev. Lett. **110**, 103601 (2013).
[48] M. Alagia, P. Candori, S. Falcinelli, M. Lavollee, F. Pirani, R. Richter, S. Stranges, and F. Vecchiocattivi, J. Phys. Chem. A **113**, 14755 (2009).
[49] A. S. Alnaser, C. M. Maharjan, X. M. Tong, B. Ulrich, P. Ranitovic, B. Shan, Z. Chang, C. D. Lin, C. L. Cocke, and I. V. Litvinyuk, Phys. Rev. A **71**, 031403(R) (2005).
[50] Y. Sato, H. Kono, S. Koseki, and Y. Fujimura, J. Am. Chem. Soc. **125**, 8019 (2003).
[51] C. Wu, G. Zhang, C. Wu, Y. Yang, X. Liu, Y. Deng, H. Liu, Y. Liu, and Q. Gong, Phys. Rev. A **85**, 063407 (2012).
[52] A. E. Slattery, T. A. Field, M. Ahmad, R. I. Hall, J. Lambourne, F. Penent, P. Lablanquie, and J. H. D. Eland, J. Chem. Phys. **122**, 084317 (2005).
[53] T. A. Field and J. H. D. Eland, Chem. Phys. Lett. **211**, 436 (1993).
[54] B. P. Tsai and J. H. D. Eland, Int. J. Mass Spectrom. Ion Phys. **36**, 143 (1980).
[55] V. Sharma, B. Bapat, J. Mondal, M. Hochlaf, K. Giri, and N. Sathyamurthy, J. Phys. Chem. A **111**, 10205 (2007).
[56] H. Hogreve, J. Phys. B **28**, L263 (1995).
[57] M. Hochlaf, F. R. Bennett, G. Chambaud, and P. Rosmus, J. Phys. B **31**, 2163 (1998).
[58] S. Miyabe, C. W. McCurdy, A. E. Orel, and T. N. Rescigno, Phys. Rev. A **79**, 053401 (2009).
[59] X. M. Tong, Z. X. Zhao, and C. D. Lin, Phys. Rev. A **66**, 033402 (2002).
[60] P. Dietrich, D. T. Strickland, M. Laberge, and P. B. Corkum, Phys. Rev. A **47**, 2305 (1993).
[61] S.-K. Son and S.-I. Chu, Phys. Rev. A **80**, 011403(R) (2009).
[62] J. Wu, L. P. H. Schmidt, M. Kunitski, M. Meckel, S. Voss, H. Sann, H. Kim, T. Jahnke, A. Czasch, and R. Dörner, Phys. Rev. Lett. **108**, 183001 (2012).
[63] S. Voss, A. S. Alnaser, X.-M. Tong, C. Maharjan, P. Ranitovic, B. Ulrich, B. Shan, Z. Chang, C. D. Lin, and C. L. Cocke, J. Phys. B: At., Mol., Opt. Phys. **37**, 4239 (2004).
[64] K. L. Reid, Mol. Phys. **110**, 131 (2012).
[65] A. S. Alnaser, S. Voss, X. M. Tong, C. M. Maharjan, P. Ranitovic, B. Ulrich, T. Osipov, B. Shan, Z. Chang, and C. L. Cocke, Phys. Rev. Lett. **93**, 113003 (2004).
[66] J. Wu, X. Gong, M. Kunitski, F. K. Amankona-Diawuo, L. P. H. Schmidt, T. Jahnke, A. Czasch, T. Seideman, and R. Dörner, Phys. Rev. Lett. **111**, 083003 (2013).